18

MgB_2 SQUID for Magnetocardiography

Yoshitomo Harada[1],
Koichiro Kobayashi[2] and Masahito Yoshizawa[2]
[1]*National Institute for Materials Science, Tsukuba,*
[2]*Graduate School of Engineering, Iwate University, Morioka,*
Japan

1. Introduction

The discovery of the superconductivity at a transition temperature (T_C) of 39 K in magnesium diboride (MgB_2) has attracted much attention from many researchers for scientific as well as technical reasons [1]. Compared with Cu-based superconductors (cuprates), MgB_2 has lower anisotropy and larger coherence length, in addition to high T_c [2]. These characteristics of MgB_2 give rise to new applications for superconductor devices that can operate in the temperature range between 20 and 30 K; examples of such devices are Josephson junctions and integrated circuits. This temperature range can be easily achieved by using economical and compact cryocoolers or liquid hydrogen. The use of cryocoolers may transform the superconductor from being specialized and advanced technology into common usage in consumer devices. In the future, hydrogen gas may be widely used for carbon-free power generation such as in fuel cells. Liquid hydrogen would be available for these purposes, and may be utilized for the cooling of low-temperature devices. In addition, MgB_2 is considered to be a clean superconducting material, using neither toxic nor rare earth elements.

Thus far, we have developed SQUID (Superconducting Quantum Interference Device) apparatuses, such as magnetocardiography (MCG) and non-destructive evaluation (NDE) systems, by using Nb and cuprates. Since the discovery of superconductivity in MgB_2 and its promising potential, we have focused our research on developing SQUID as well as a high-frequency filter made of MgB_2. As a first step, we developed a synthesis method for high-quality films, which is the basis of fabrication of such devices. Next, since 2004, we have been working on developing a SQUID and a high-frequency filter device. Finally, we succeeded in measuring the magnetic signal from a human being (MCG signal) by using MgB_2 SQUID with a specially developed control circuit (digital FLL). In this article, we discuss our achievements and progress on the development of superconducting devices using MgB_2 films.

2. Synthesis of high-quality films

Synthesis of high-quality film is a key technology in developing superconductor devices. We would first like to introduce various synthesis methods for MgB_2 films. There have already been many reports on the techniques that have been used far for the preparation of MgB_2

thin films. These preparation methods can be categorized into two types: post-annealing methods and as-grown methods.

We will now introduce the post-annealing method. First, Mg and B together or MgB_X alone are evaporated on the substrates at room temperature in this method. Second, these films are annealed inside an electric furnace in an atmosphere of Mg gas. This process improves the physical properties so that and we can obtain superconducting behavior [3,4]. This method is characterized by achieving a high T_C through high-temperature annealing. However, this method is not preferred for the synthesis of the films used in the devices due to the occurrence of the interfacial reactions and the degradation of the surface flatness by high-temperature annealing.

On the other hand, the as-grown method does not need an annealing process. The as-grown method is suitable for the fabrication of superconducting devices because it provides a flat surface. To date, several groups have reported the synthesis of as-grown superconducting MgB_2 films. In particular, the HPCVD (hybrid physical chemical vapor deposition) [5] method and the MBE (molecular beam epitaxy) method [6-9] have achieved high T_c values that are over 30 K. The HPCVD method, which enables a high-temperature growth process of the film at about 1000 K, succeeded in synthesizing the film with a high T_C value of 39 K by using Mg that has a high degree of volatility.

In contrast to HPCVD, the MBE method adopts a low synthesis temperature of about 573 K and is carried out in a high vacuum. The T_C of MgB_2 films grown by the MBE method is relatively lower than that obtained from other methods and is limited to be around 34 K. The growth conditions for the MBE method adopted by the research groups other than our group are, however, high growth rate and high substrate temperature. The high growth rate compensates for the deficiency of Mg through re-evaporation due to its volatility and prevents the oxidation of Mg. This concept is very similar to that of the HPCVD method. High deposition rate and high growth temperature have been a mainstay in the fabrication of the high-quality MgB_2 films.

We adopted a low substrate temperature, a low deposition rate, and an ultra-high vacuum to obtain high-quality MgB_2 films. The characteristic feature of the MBE method is low-temperature synthesis. According to Liu *et al*., MgB_2 is synthesized in a wider temperature range, particularly at low temperatures, as the vacuum increases [10]. The growth at low temperature reduces the re-evaporation of Mg. The deposition rate and the supply of Mg and B have to be reduced due to the super-saturation of Mg. Under these conditions, Mg may be oxidized. However, the ultra-high vacuum in an MBE apparatus prevents the oxidation and permits the growth of high-quality films.

In terms of synthesis conditions, our method is conceptually opposite to the conventional fabrication methods for MgB_2 films. Figure 1 shows the typical temperature dependence of the resistivity curves of MgB_2 films fabricated by our method. The growth temperature was set as 473 K, which is about 100 K lower than that in other reports. In our method, the range of the deposition temperature was between 373 K and 523 K. This is the same range as that in the phase-diagram of Lie *et al.* and may be obtained by extrapolating the pressure range to 10^{-7} Pa and 10^{-8} Pa. The *T*c of the sample in Fig. 1 was 32 K, and the transition width is smaller than 1.0 K. In our method, T_c can reach a value of up to 37 K by the adoption of various additional process improvements, which will be presented later.

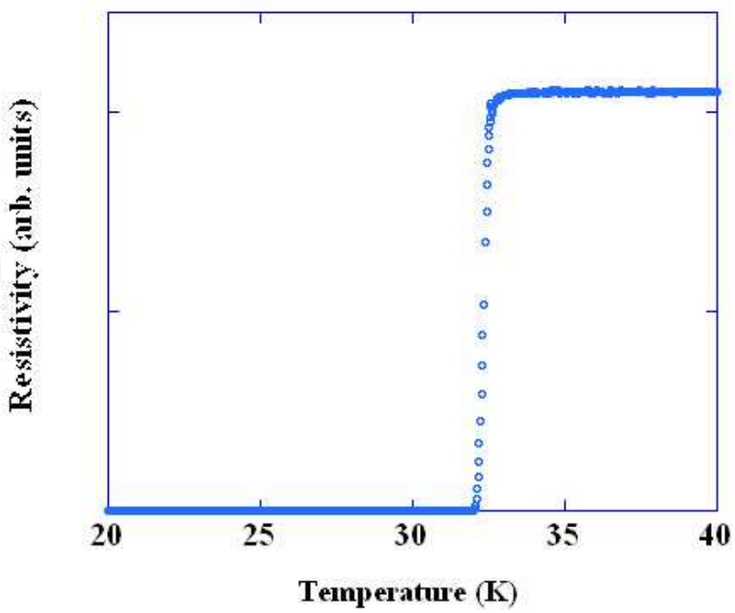

Fig. 1. Temperature dependence of the resistivity of MgB_2 films.

Figure 2 shows the critical current density (J_C) of MgB_2 films as a function of temperature. The measurement was carried out using patterned micro-bridges, which were made by standard photo-lithography and the Ar ion beam milling method. The inset of Fig. 2 is an optical microscope image of the MgB_2 micro-bridge. The dimensions of the micro-bridge were 10 μm (width) × 30 μm (length). The electrical contact was made by gold wire directly bonded to a Cu/MgB_2 contact pad using silver paste. The highest value of J_c is 11.6 MA/cm² at 4.2 K on an MgO (100) substrate. The $J_C(0)$ value is 12.5 MA/cm². This value is considered to be very high for MgB_2 films.

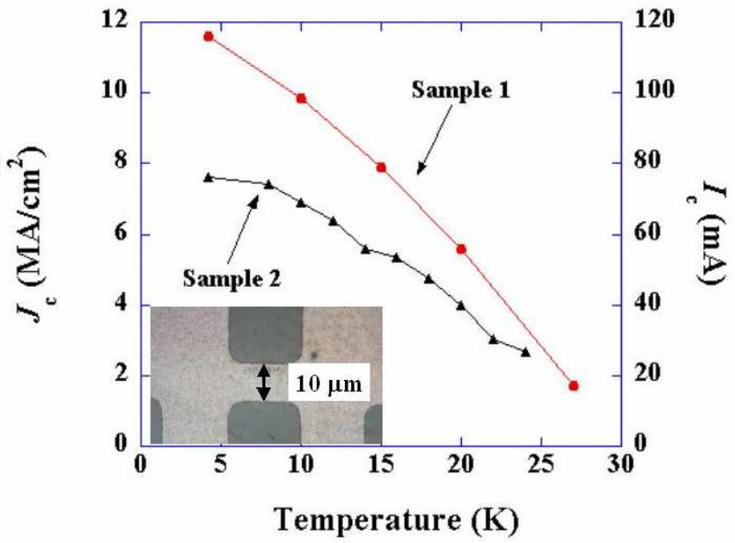

Fig. 2. Temperature dependence of the critical current density (J_C) of MgB_2 micro-bridge. J_C is calculated from the critical current (I_C).

We will discuss the reason why the J_C of our sample synthesized on an MgO substrate is so high. From AFM and SEM measurements, the grain size of MgB_2 films on MgO substrates is 20-50 nm. This value is smaller than that on an Al_2O_3 or Si substrate. The mismatch between the in-plane lattice constant of MgB_2 and MgO is 26.7 %. MgO (100) plane has a square surface structure, whereas MgB_2 has a hexagonal surface structure. These conditions led to a smaller grain size of MgB_2 when it is deposited on MgO. The grain shape of MgB_2 is of the columnar-type, and the grain boundaries work as effective pinning centers. Therefore, the smaller grain size provides more pinning centers and leads to high values of J_C in the perpendicular field.

Next, we tried to further improve the quality of the grown MgB_2 films such that they can be used for the fabrication of superconducting devices. According to the works of Shimane University [11] and NICT [12], the in-plane lattice matching between MgB_2 and the substrate plays an important role in the growth of high-quality MgB_2 films using the MBE method.

The structural quality of MgB_2 films was improved by using AlN ($\Delta d = 1.9\%$) and TiZr ($\Delta d = 3.6\%$) buffer layers having lattice constants close to that of MgB_2. We initially employed ZnO (0001) as the substrate as its substrate closely matched that of MgB_2. The in-plane lattice spacing of the hexagonal ZnO lattice (a = 0.3522 nm) is close to that of the MgB_2 lattice ($\Delta d = 5.4\%$; Δd of Al_2O_3, for example, is 35.2 %) [13]. However, we could not do an in-plane alignment for these films, although their T_c is relatively high at 35 K. The cross-sectional transmission electron microscope (TEM) image showed a large amount of reaction products near the MgB_2/ZnO interface. In addition, intermixing between Zn and MgO was observed near the MgB_2/ZnO boundary, which is ascribed to the free energy difference between the substrate and the film. The free energy of MgO is -547.1 kJ/mol and is lower than the value of -303.3 kJ/mol for ZnO. Therefore, Zn in ZnO is easily replaced by Mg, and MgO is formed.

The best-quality MgB_2 film was obtained by adopting titanium (Ti) film as a buffer layer on a ZnO substrate, which was fabricated by evaporation using an electron-beam gun cell in an MBE chamber [14]. Figure 3 shows the superconducting properties of MgB_2 films when a 15 nm Ti buffer layer is adopted. When the MgB_2 film was deposited on a ZnO (0001) substrate, the T_C increased from 33 K to 36K with the insertion of a Ti buffer layer. By using *in situ* reflection high-energy electron diffraction (RHEED), Ti buffer layers were grown epitaxially in the configurations Ti (0001) || ZnO (0001) and Ti $\left[1\bar{1}00\right]$ || ZnO $\left[11\bar{2}0\right]$. The in-plane orientation (ϕ) scans of the $11\bar{2}2$ reflections around the c-axis of the MgB_2 films are shown in Fig. 4, wherein two sets of 6-fold symmetric peaks appear at intervals of every 60°. The peak sets corresponds to two types of domains rotated by 30° from each other about the c-axis. Furthermore, we found that one set of the peaks increased in highest and became predominant with increasing thickness of the Ti buffer layer. This result indicates that the in-plane alignment of the MgB_2 lattice is improved by the presence of the Ti buffer layer.

Nishidate *et al.* investigated the effect of the Ti buffer layer on ZnO substrates prior to the deposition of Mg and B by studying and calculating its molecular dynamics (MD) [15]. Because Ti atoms occupy a particular adsorption point, Mg adsorption was limited on a metal oxide substrate and Mg is used in the formation of MgB_2. In addition, the lattice constant of Ti, a = 0.295 nm, matches that of MgB_2, and the free energy of -849.89 kJ/mol for Ti-O is lower than the corresponding values for both MgO and ZnO. Ti also hinders the formation of MgO.

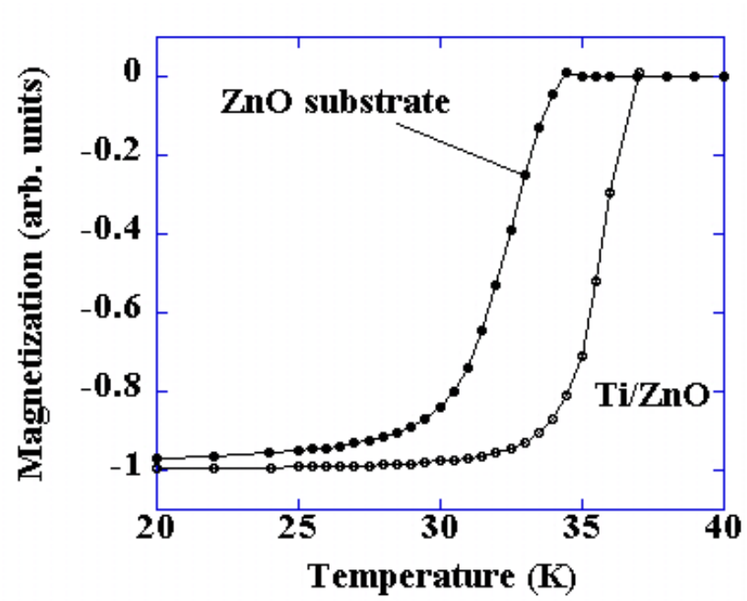

Fig. 3. Temperature dependence of the magnetization of MgB_2 film on the ZnO and Ti/ZnO substrate.

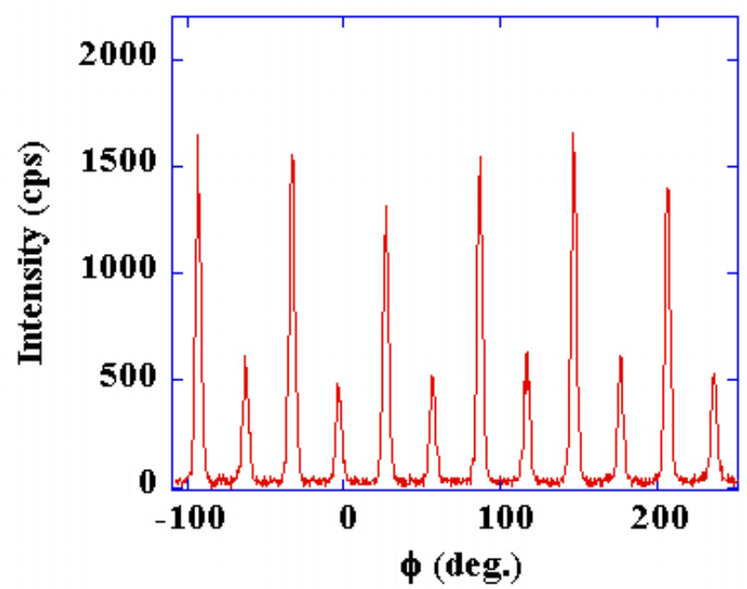

Fig. 4. XRD ϕ scan image of MgB_2 $11\bar{2}2$ peaks from MgB_2/Ti films deposited on ZnO substrate.

We achieved a value of T_C = 37 K by the MBE method, which is the same as that with HPCVD. Fujiyoshi *et al.* report that the J_C of the MgB_2 films on the Ti buffer layer is higher than that of MgB_2 on the substrates [16]. Therefore, the pinning force due to the grain boundaries at the MgB_2 film on the Ti buffer layer is stronger than that of other films.

3. Implementation of Josephson junction and SQUID by lithography technique

There are three types of Josephson junction fabrication methods for SQUID and they are as follows: SIS tunneling junctions, nano-bridge junctions and SNS junctions. The first tunneling MgB_2 junctions were fabricated by the NTT group [17]. We have developed and used an SIS junction [18]. Subsequently, both the Twente University and European groups succeeded in the fabrication of nano-bridge MgB_2 junctions [19]. We have developed nano-bridge MgB_2 SQUIDs devices that are optimized for MCG measurement, which are based on the design of the Twente University group. Nano-bridge junctions were made using focused ion beam (FIB) milling apparatus. Detailed fabrication conditions are reported elsewhere [20]. Figure 5(a) shows the layout of the MgB_2-SQUID device in this experiment. Figure 5(b) shows the scanning ion microscope (SIM) image of the nano-bridge junctions. We designed the size of junction to be 200 nm wide and 200 nm in length. From the SIM image, we observed that the actual junction size matched the design expectations very close.

Figure 6 (a) shows the voltage modulation (ϕ–V curve) of the nano-bridge MgB_2 SQUIDs at 24.4 K. Figure 6 (b) is the I-V curve for this SQUID. The voltage modulation due to the applied magnetic field can be seen to increase with decreasing temperature. An approximate magnitude of 22 μV is recorded at 20 K. The bias current applied was tuned to get the largest voltage modulation; the bias current value was 2280 μA for this sample, giving rise to the maximum modulation of 18.47 μV.

Figure 7 shows the ϕ-V curve of other SQUID with the same nano-bridge size. The measurement temperature is set to 20.81 K. The voltage modulation was measured for the bias current from 2550 to 2585 μV. The maximum modulation voltage was 33.55 μV when the bias current was set to be 2577 μA. The external magnetic field density corresponding to the magnetic flux quantum was 11.4 nT. The measured effective SQUID area (A_{eff}) was estimated to be 0.18 mm².

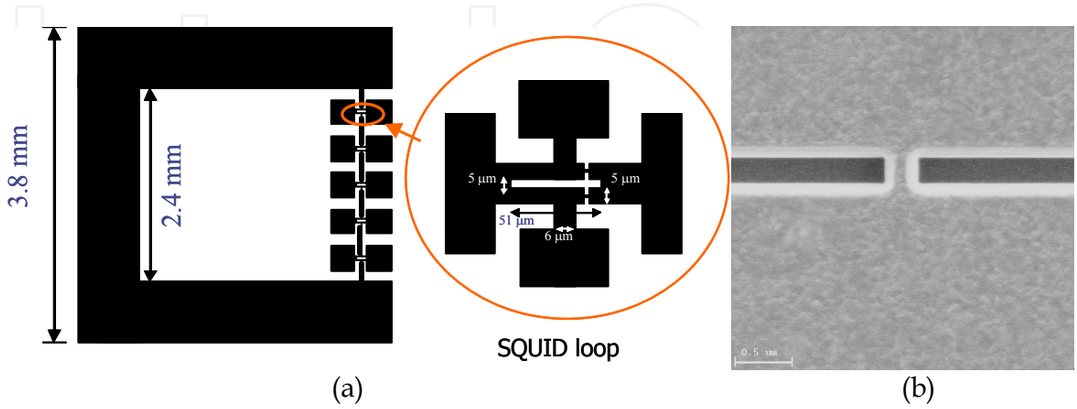

Fig. 5. (a) Layout of an MgB_2-SQUID device. (b) FIB-SIM image of nano-bridge junctions. The size of nano-bridge is 200 nm wide and 200 nm long.

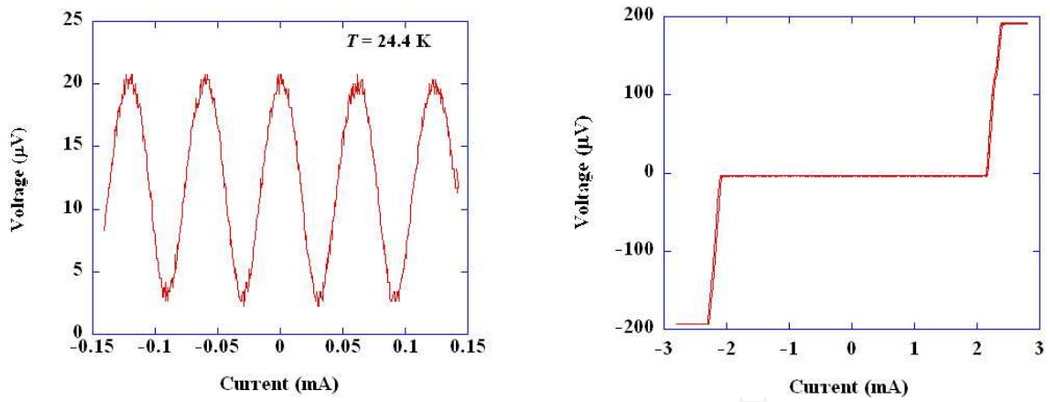

(a) (b)

Fig. 6. SQUID characteristics of 200 nm nano-bridge type MgB_2-SQUID. (a)Voltage modulation, (b) *I-V* property.

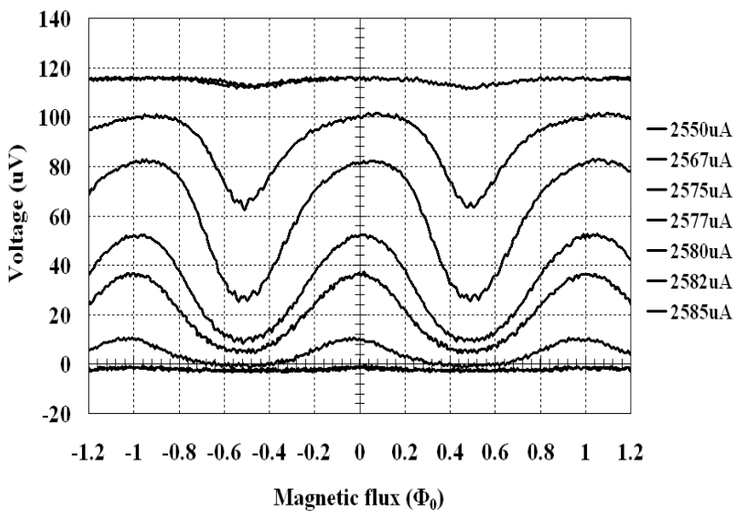

Fig. 7. Magnetic flux dependence of voltage modulation of an MgB_2-SQUID with various bias currents.

We encountered two problems during the development of SQUID. One is the reduction of the yield ratio, due to the small size of the nano-bridge, which is close to the size limitation of the FIB fabrication process. Another is the hysteretic behavior of the *I-V* curve at the transition edge, which appears at low temperatures. This causes instability in the bias current and makes measurements very difficult. The first problem was solved by adopting thinner films. We are able to obtain *I-V* and ϕ-*V* properties and even expand the width of the nano-bridge by decreasing film thickness. At present, we retain a high yield of about 90 % for the fabrication of 65 nm thick film and the 400 nm wide nano-bridges. The second problem was resolved by placing a resistor in parallel to the MgB_2 nano-bridges. We were able to eliminate the effect of hysteresis by inserting the resistor.

4. SQUID electronics

The input-output (Φ - V) characteristic of SQUID is nonlinear as shown in Fig. 8. A sinusoidal output voltage with the appropriate periodicity is generated, when a magnetic flux is applied in SQUID. A control circuit, known as the FLL (flux locked loop) circuit, is necessary to linearize the input-output characteristic so that the SQUID can be utilized as a magnetic sensor. An example of such an FLL circuit is shown in Fig. 9. The FLL circuit provides the feedback necessary to fix the output at the defined value (the lock point) in a sinusoidal SQUID output. Then, by using only the small area in the vicinity of the lock point, we get the desired linear output. The external magnetic field applied to a pick-up coil produces the voltage in the SQUID. The EMF-voltage is amplified, integrated and then fed back to SQUID in order to maintain to the lock point. Then the applied magnetic field is nullified. This integrated value becomes the output signal of the FLL circuit, and it is equal to the input magnetic signal applied to the pick-up coil.

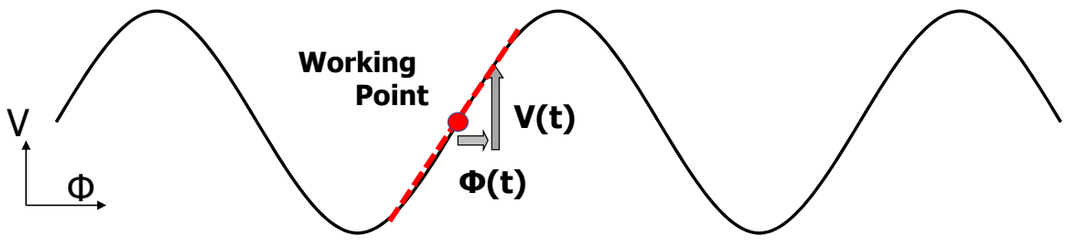

Fig. 8. Input-output (Φ - V) characteristic of SQUID.

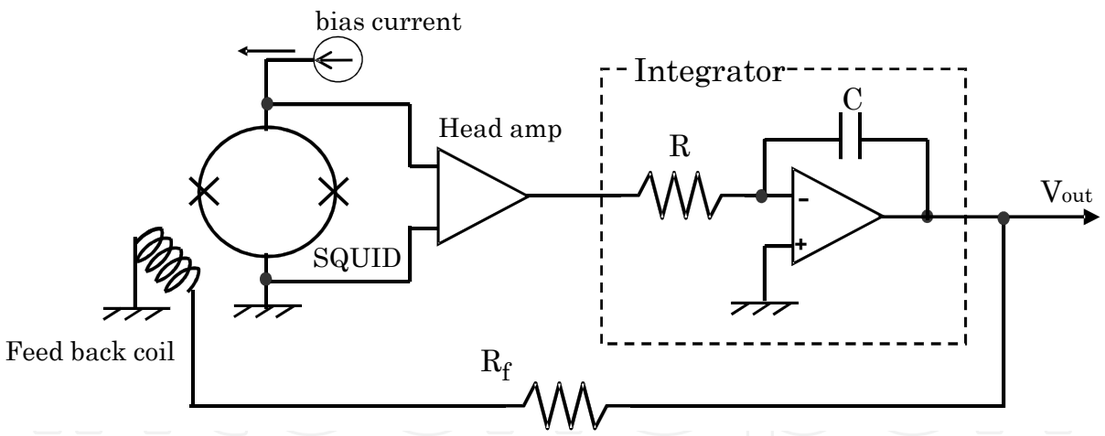

Fig. 9. Example of the FLL circuit

In recent years, it has been shown by several groups that the electronics within the digital SQUID, where the flux-locked loop system is controlled by a digital circuit, can achieve a wide dynamic range [21-23]. These FLL systems can measure biomagnetic signals in a magnetically unshielded environment. We call a digitally controlled flux-locked loop system (D-FLL).

A D-FLL system satisfies unshielded conditions: its dynamic range is expanded by jumping to a lock point on the SQUID's periodic Φ-V characteristic and by keeping a count of the number of such events. This method was named flux-quanta counting (FQC) [24, 25]. The

integrator of the D-FLL is reset every time the feedback flux exceeds ±1 Φ_0 and the corresponding Φ_0 steps are counted. Usually, the original input flux is reconstructed on a digital signal processor that is a part of the FLL circuit. The dynamic range depends on the architecture of the digital signal processor, which is typically 32-bit. Furthermore, high-speed signal processing makes a digital feedback loop delay shorter. A high-performance digital signal processor is required to increase the dynamic range and slew rate. So far, it has proven difficult to make a high performance system with the typical single-chip microcontroller that is generally used in such circuits.

We have developed a double-counter equipped D-FLL system in Fig. 10. The double-counter method has two counters on a single-chip microcontroller and a host computer. The digital integrator unit calculates feedback flux data. If feedback flux exceeds ±0.5Φ_0, the integrator unit subtracts 1 Φ_0 from the digital integrator data or adds 1 Φ_0 to it, instead of resetting the FLL. The feedback loop process works more quickly than the data transmission from the one-chip microcontroller into a host computer. The integrator data and Couner1 data is sent at periodic time intervals defined by a timer. Counter1 is reset every time after this transmission is complete and commences the count of Φ_0 steps during the next interval. Counter2 integrates the data transmitted from Counter1. The host computer reconstructs the measured flux data using Counter2 as well as integrator data. Because a host computer reconstructs input flux, the workload of the single-chip microcontroller is decreased, leading to a quicker operation of the feedback loop than that of the system without a double-counter method. The high-performance D-FLL system using a single-chip microcontroller is achieved by a method that employs two counters.

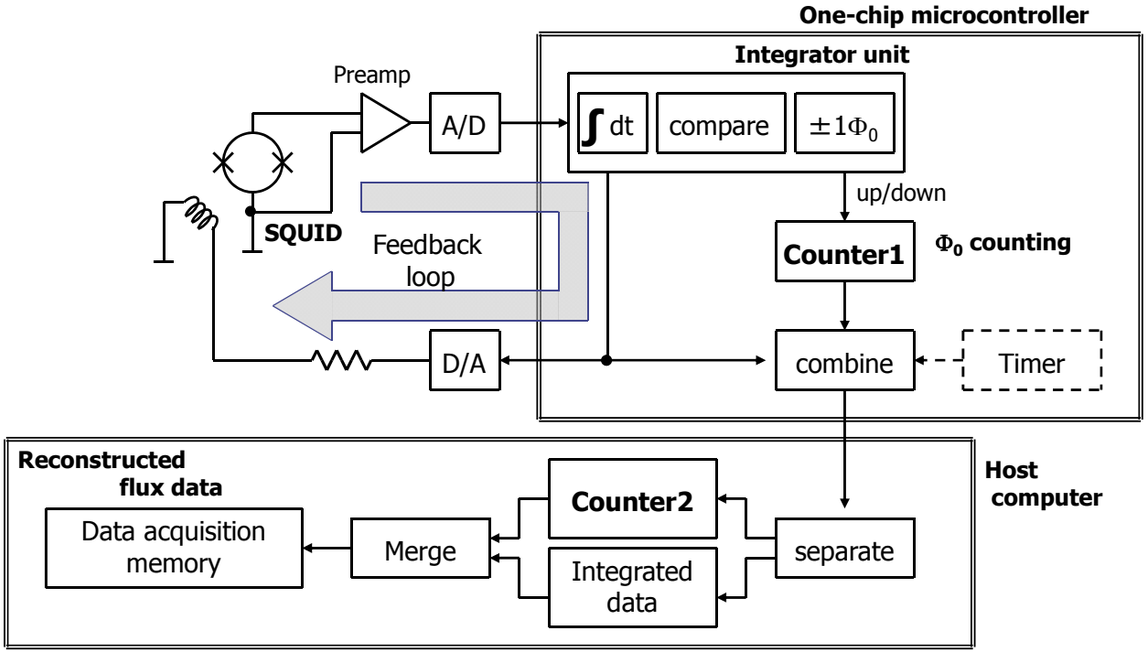

Fig. 10. Block diagram of the double-counter D-FLL system.

Our latest D-FLL system is composed of a commonly used 8-bit single-chip microcontroller, a 12-bit A/D converter, two 16-bit D/A converters and some other inexpensive and easily

obtained devices [26]. The measured magnetic flux data is recorded at the rate of 1 kHz via an RS-232 interface. The time delay of the digital feedback loop is 8.4 μs. The first-order gradiometer is made of a low-T_c dc SQUID (niobium:Nb), has a pickup coil with a diameter of 17.8 mm and a baseline of 50 mm, and was used for the characteristic evaluations of the D-FLL system. The sensitivity which is calculated using the relation B/Φ_0 = 0.6 nT/μΦ_0, where B is the flux density in the pickup coil, gives a measure of the flux resolution of 11.35 fT/digit (19 μΦ_0/digit) for this system.

Figure 11 shows an active area of the D-FLL system. The terminology "active area" means that the system can measure magnetic signals just in this area. The right vertical axis is shown as a dynamic range when a 16-bit D/A converter is used for about 1 Φ_0 feedback flux. The measured dynamic range is 218 Φ_0 (141 dB) at 1 Hz, 22 Φ_0 (121 dB) at 10 Hz, and 2.1 Φ_0 (100 dB) at 100 Hz. In addition, the measured slew rate is 1.3 kΦ_0/s. The D-FLL system can operate in a stable manner if power line noise that is usually the main problem encountered with unshielded operations is less than 4.1 Φ_0 in amplitude at 50 Hz.

Figure 12 shows the measured D-FLL output noise spectra both inside and outside a magnetically shielded room (MSR). The lower line is measured in the MSR and the upper line is measured in an unshielded environment. The white noise level used was 36.1 fT/Hz$^{1/2}$ and the 1/f corner frequency was 2 Hz in an MSR. The noise spectrum measured outside an MSR contained some unidentified noises beside power line noise that exhibited 465 pT/Hz$^{1/2}$ (0.78 Φ_0/Hz$^{1/2}$) at 50 Hz.

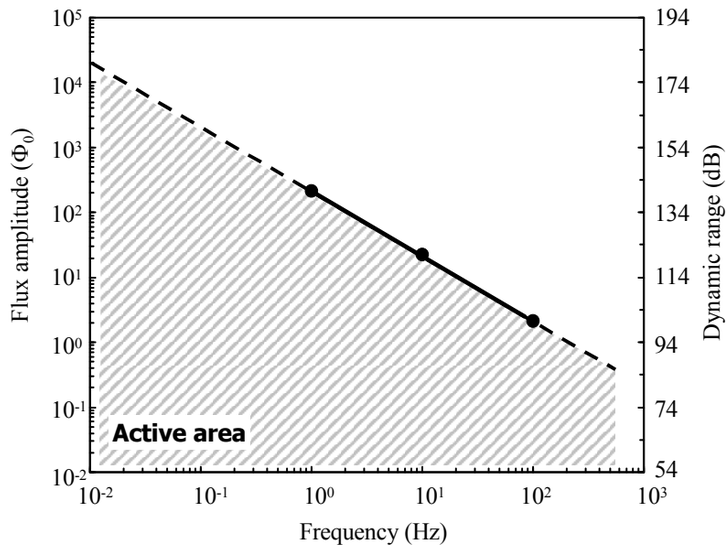

Fig. 11. Active area of the D-FLL system. An "active area" implies that the system can measure magnetic signal just in this area. The right vertical axis is shown as a dynamic range when 16 bit D/A converter is used for 1 Φ_0 feedback flux.

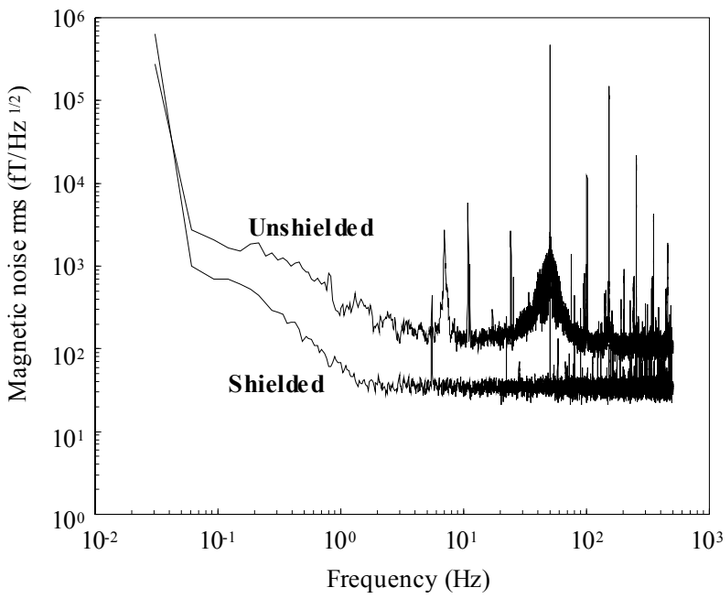

Fig. 12. Magnetic noise spectra measured in an MSR. The lower line is the measurement in an MSR and the upper line is from an unshielded environment.

5. Magnetocardiogram measurements

SQUIDs have been utilized for the detection of weak magnetic fields in our daily life from non-distraction evaluation to bio-magnetic field detection. Recently, the magnetocardiography (MCG) has attracted much attention as a potential application of SQUID, because MCG systems with SQUID provide higher sensitivity than other systems and because cardiac diagnosis plays an important role in the prevention of heart disease. Thus far, we have developed a multi-channel MCG system by using Nb SQUID [27]. Following that effort, we developed a conventional MCG system made of MgB_2.

Figure 13 shows the block diagram of a cryocooler system and the close-up of a cold cylinder. A commercially available pulse-tube cooler (Sumitomo RP-052D) was used. The cold head of the cryocooler is connected to the compressor via a valve unit. Because the valve unit produces magnetic noise, the cold head and the refrigerator component are installed in an MSR, and the valve unit is set outside of it. They are connected by a long copper tube.

The mechanical vibration of the refrigerator is ±3 μm at 1.2 Hz. The cold stage is connected to the refrigerator by a copper column to enable refrigeration. The distance between them is 608 mm.

This refrigerator can achieve a temperature of about 5 K without a load. Our cryocooler has two modes. The first mode is the SQUIDs characterization mode. This is used for characterization of MgB_2 SQUIDs. The cold stage and the cold cylinder are covered by a radiation shield, which is made of copper and has a thickness of 3.4 mm. The MgB_2 SQUID is set underneath the cold stage. The lowest temperature in this mode was 5.6 K.

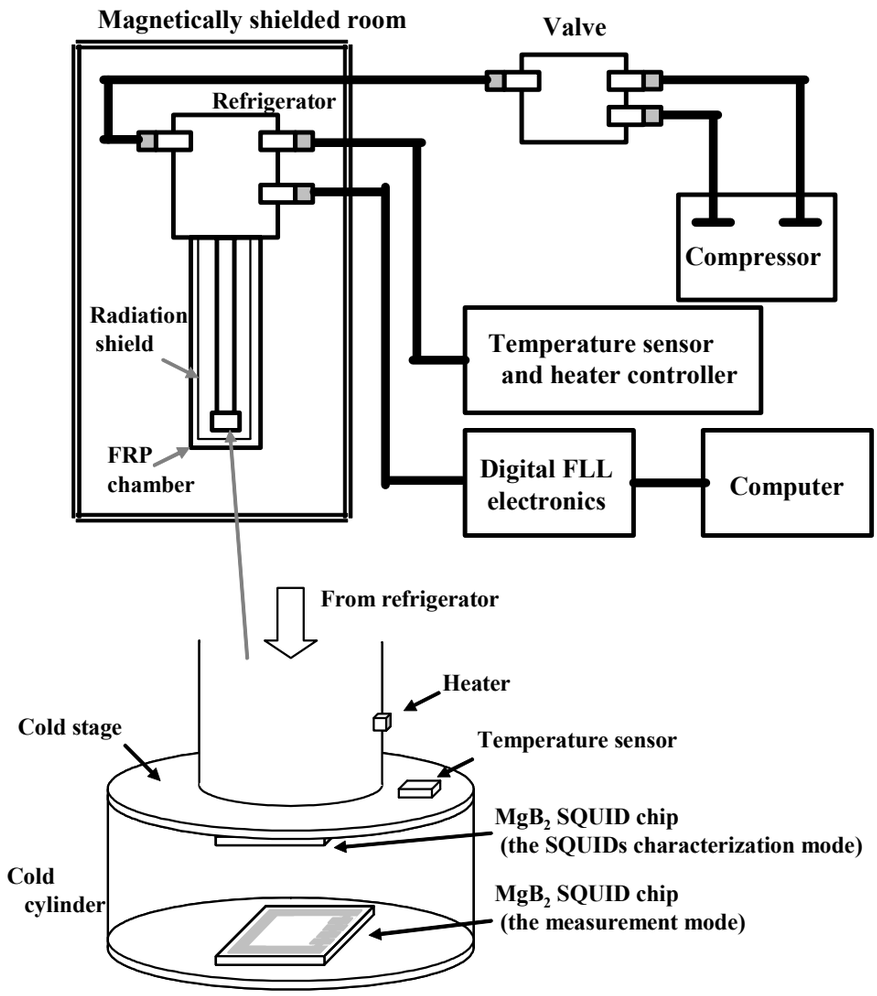

Fig. 13. Block diagram of a cryocooler system and the close-up of a cold cylinder. The MgB_2 SQUID is set under the cold stage or on the bottom plate of the cold cylinder when the system is used in either the SQUIDs characterization mode or the measurement mode.

The second mode is the measurement mode. This mode is used for measurement of an external magnetic field, as in the case of MCG. The cold stage and the cold cylinder are covered by super insulation films instead of a radiation shield. The MgB_2 SQUID is set on the bottom plate of the cold cylinder and has a thickness of 2.0 mm. The lowest temperature achieved in this mode was 11.9 K. A temperature sensor and a heater are placed on the cold stage and the column, respectively. They are connected to a PID controller, with which the temperature of the cold stage is controlled. Both the SQUID characterization mode and the measurement mode are controlled and operated by a computer through the D-FLL electronics.

Figure 14 shows the magnetic flux noise spectrum measured inside a single layer MSR. The white magnetic flux noise was 6.8 $pT/Hz^{1/2}$. The largest peak was caused by power lines of 50 Hz. Other peaks were observed at 1.2 Hz and its harmonics of that frequency. They were caused by the refrigerator and had a magnitude of 13.8 pT at 1.2 Hz.

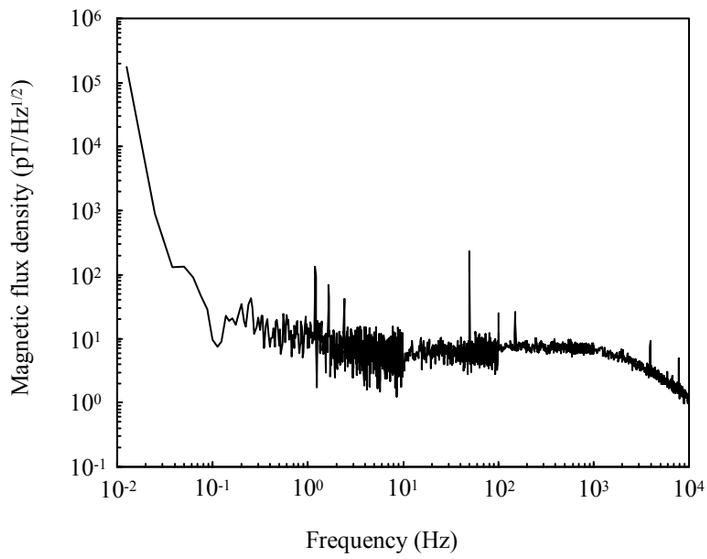

Fig. 14. Magnetic noise spectrum of the system measured inside an MSR.

Figure 15 shows the photograph of the actual measurement and the MgB_2 magnetometer that was used in the experiments. The magnetocardiogram was measured by our MgB_2 SQUID system inside the MSR. This measuring apparatus was cooled by a pulse tube refrigerator instead of liquid helium.

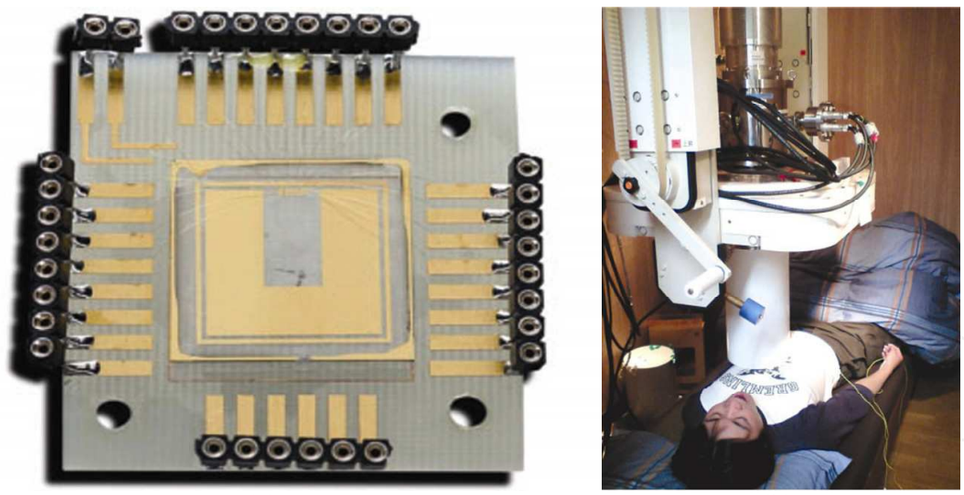

(a) (b)

Fig. 15. Photographs of the MgB_2-SQUID device and magnetocardiogram measurements.

Figure 16 shows a magnetocardiogram waveform of a healthy volunteer. This waveform was obtained by applying a digital low-pass filter whose cutoff frequency was 40 Hz and the waveform was averaged over 536 measurements [28]. We have succeeded in measuring the QRS complex and the T wave which is characterized in the activity of the human heart. This result shows a possible practical use of the MgB_2-SQUID MCG system cooled by refrigeration above 20 K without liquid cryogen, although the system is still under development.

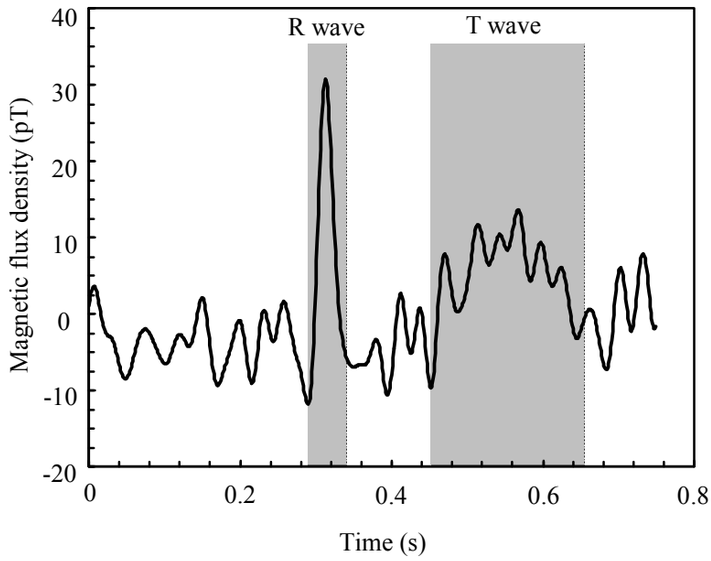

Fig. 16. Magnetocardiogram waveform measured by the MgB_2 SQUID system inside an MSR. The waveform was obtained by applying a software low-pass filter (40Hz) and 536 times averaging.

6. Summary

We built a prototype of a nano-bridge type MgB_2 SQUID device and optimized it for the measurement of magnetocardiogram. The results indicate that our method for the fabrication of SQUID of an MgB_2 magnetometer optimized for MCG measurement is effective. We are currently conducting research to reduce the noise from the refrigerator and to optimize the MgB_2 SQUID MCG system. A multi-channel type MCG system is also under development. The crystalline characteristics of MgB_2 films should be further improved to obtain better device performance. In the near future, the MgB_2 SQUID device is expected to have excellent performance. In addition to the SQUID device, we developed a high-frequency filter device. The detailed results of the filter device are shown in the papers of co-workers at Yamagata University [29]. Figure 17 shows the photographs of the filter device that was developed and studied.

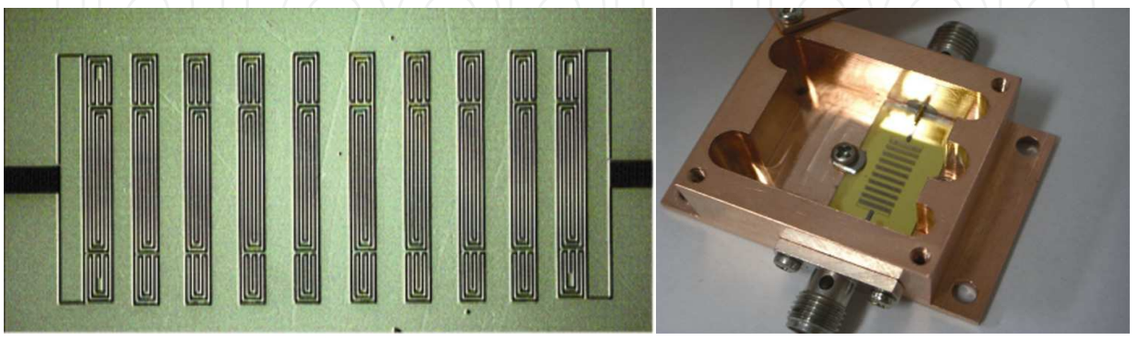

(a) (b)

Fig. 17. Photographs of the high-frequency filter device. The filter device was mounted on a Cu cavity.

7. Acknowledgments

The authors thank H. Yamaguchi, Y. Fujine, D. Oyama, K. Ikeda, S. Goto, T. Nakajima, T. Takahashi, H. Iriuda, T. Oba, A. Okubo, J. Araaki, K. Meguro, T. Abe, H. Endo, Y. Uchikawa and K. Fujisawa for the cooperation of MgB_2 SQUID project, and M. Iitake for his technical assistance of FIB process. This work was supported by the Japan Science and Technology Agency. A part of this work was conducted at the AIST Nano-Processing Facility, supported by "Nanotechnology Network Japan" of the Ministry of Education, Culture, Sports, Science and Technology (MEXT), Japan.

8. References

[1] Nagamatsu, J., Nakagawa, N., Muranaka, T., Zenitani, Y. & Akimitsu, J. (2001). Superconductivity at 39K in magnesium diboride, *Nature* 410: 53.

[2] Buzea, C. & Yamashita, T. (2001). Review of the superconducting properties of MgB_2, *Supercond. Sci. Technol.* 14: R115.

[3] Kang, W. N., Kim, H. J., Choi, E. M., Jung, C. U. & Lee, S. I. (2001). MgB_2 superconducting thin films with a transition temperature of 39 Kelvin, *Science* 292: 1521.

[4] Eom, C. B., Lee, M. K., Choi, J. H., Belenky, J. J., Song, X., Colley, L. D., Naus, M. T., Patnaik, S., Jiang, J. J., Rikel, M., Polyanskii, A., Gurevich, A., Cai, X. Y., Bu, S. D., Babcock, S. E., Hellstrom, E. E., Larbalestier, D. C., Rogado, N., Regan, K. A., Hayward, M. A., He, T., Slusky, J. S., Inumaru, K., Haas, M. K. & Cava, R. J. (2001). Thin film magnesium boride superconductor with very high critical current density and enhanced irreversibility field, *Nature* 411: 558.

[5] Zeng, X., Pogrebnyakov, A. V., Kotcharov, A., Jones, J. E., Xi, X. X., Lysczek, E. M., Redwing, J. M., Xu, S., Li, Q., Lettieri, J., Schlom, D. G., Tian, W., Pan,X. & Liu, Z. K. (2002). In situ epitaxial MgB_2 thin films for superconducting electronics, *Nature Mater.* 1: 35.

[6] Ueda, K. & Naito, M. (2003). In situ growth of superconducting MgB_2 thin films by molecular beam epitaxy, *J. Appl. Phys.* 93: 2113.

[7] Jo, W., Huh, J.-H., Ohnishi, T., Marshall, A. F., Beasley, M. R. & Hammond, R. H. (2002). In situ growth of superconducting MgB_2 thin films with preferential orientation by molecular beam epitaxy, *Appl. Phys. Lett.* 80: 3563.

[8] Erven, A. J., Kim, T. H., Muenzenberg, M. & Moodera, J. S. (2002). Highly crystallized as-grown smooth and superconducting MgB_2 films by molecular beam epitaxy, *Appl. Phys. Lett.* 81: 4982.

[9] Kobayashi, Y., Doi, T., Kitaguchi, H., Okuzono, M., Nagatomo, K., Hamada, S. & Hakuraku, Y. (2005). Preparation of MgB_2 thin films by an electron-beam evaporation technique and post-annealing effect on the as-grown films, *TEION KOGAKU* 40: 7 (in Japanese).

[10] Liu, Z.-K., Schlom, D. G., Li, Q. & Xi, X. X. (2001). As-grown superconducting MgB_2 thin films prepared by molecular beam epitaxy, *Appl. Phys. Lett.* 78: 3678.

[11] Sakata, O., Kimura, S., Tanaka, M., Yata, S., Kato, T., Yamanaka, K., Yamada, Y., Matsushita, A. & Kubo, S. (2004). High-quality as-grown MgB_2 thin-films fabrication at a low substrate temperature using an in-plane-lattice near-matched epitaxial-buffer-layer. *J. Appl. Phys.* 96: 3580.

[12] Tsujimoto, K., Shimakage, H., Wang, Z. & Kaya, N. (2005). Crystallinity and superconductivity of as-grown MgB_2 thin films with AlN buffer layers, *Physica C* 426-431: 1464.

[13] Harada, Y., Takahashi, T., Kuroha, M., Iriuda, H., Nakanishi, Y., Izumida, H., Endo, H. & Yoshizawa, M. (2006). Fabrication of as-grown MgB_2 films on ZnO (0001) substrates by molecular beam epitaxy, *Physica C* 445-448: 884.

[14] Harada, Y., Yamaguchi, H., Oba, Y., Fujine, Y., Goto, S., Iriuda, H. & Yoshizawa, M. (2007). Novel stage in fabrication of as-grown MgB_2 films by adopting Ti seed layer, *Physica C* 463-465: 945.

[15] Nishidate, K., Yoshizawa, M. & Hasegawa, M. (2008). Energetics of Mg and B adsorption on polar zinc oxide surfaces from first principles, *Phys. Rev. B* 77: 035330.

[16] Haruta, M., Fujiyoshi, T., Kihara, S., Sueyoshi, T., Miyahara, K., Harada, Y., Yoshizawa, M., Takahashi, T., Iriuda, H., Oba, T., Awaji, S., Watanabe, K. & Miyagawa, R. (2007). High critical current density under magnetic fields in as-grown MgB_2 thin films deposited by molecular-beam epitaxy," Supercond. Sci. Technol. 20 (2007) L1.

[17] Ueda, K. & Naito, M. (2004). Tunnel junctions on as-grown MgB_2 films, *Physica C* 408–410: 134.

[18] Oba, T., Goto, S., Sasaki, S., Nakanishi, Y., Fujino, Y., Harada, Y., Nakamura, M., Saito, A. & Yoshizawa, M. (2008). Fabrication of all-MgB_2 Josephson junctions using MgO insulator layer, *Physica C: Superconductivity* 468: 1892.

[19] Gonnelli, R. S., Daghere, D., Calzolari, A., Ummarino, G. A., Tortello, M., Stepanov, V. A., Zhigadlo, N. D., Rogacki, K., Portesi, C., Monticone, E., Mijatovic, D., Veldhuis, D. & Brinkman, A. (2006). Recent achievements in MgB_2 physics and applications: A large-area SQUID magnetometer and point-contact spectroscopy measurements, *Physica C* 435: 59.

[20] Harada, Y., Oyama, D., Fujine, Y., Goto, S., Ikeda, K., Nakashima, T., Meguro, K., Kobayashi, K. & Yoshizawa, M. (2008). Fabrication of DC-SQUIDs of As-grown MgB_2 films, *TEION KOGAKU* 43: 354 (in Japanese).

[21] Drung, D. (2003). High- Tc and low-Tc dc SQUID electronics, *Supercond. Sci. Technol.* 16: 1320.

[22] Ludwig, C., Kessler, C., Steinfort, A. J. & Ludwig, W. (2001). Versatile high performance digital SQUID electronics, *IEEE Trans. Appl. Supercond.* 11: 1122.

[23] Schurig, T., Drung, D., Bechstein, S., Beyer, J. & Ludwig, F. (2002). High-Tc superconductor dc SQUIDs for unshielded operation and their applications, *Physica C*, 378-381: 1378.

[24] Vrba, J., Betts, K., Burbank, M., Cheung, T., Fife, A. A., Haid, G., Kubik, P. R. & Weinberg, H. (1993). Whole cortex, 64 channel SQUID biomagnetometer system, *IEEE Trans. Appl. Supercond.* 3: 878.

[25] Vrba, J. (1996). SQUID gradiometers in real environments SQUID Sensors: Fundamentals, Fabrication and Applications, (NATO ASI Series E329) ed H. Weinstock (Dordrecht: Kluwer) 117.

[26] Oyama, D., Kobayashi, K., Yoshizawa, M. and Uchikawa, Y. (2006). Development of digital FLL system for SQUID using double counter method, *IEEE Transactions on Magnetics* 42: 3539.

[27] Yoshizawa, M., He, D. F., Nakai, K., Kobayashi, K., Nakamura, Y., Yaegashi, M., Ito, M., Yashiro, H., Daibo, M., Simizu, T., Uchikawa, Y. & Noto, K. (2005). Application of SQUIDs in Iwate CREATE project, *Physica C* 426-431: 1572.

[28] Oyama, D., Harada, Y., Fujine, Y., Kobayashi, K., Uchikawa, Y. & Yoshizawa, M. (2009). Detection of MCG signal by using MgB_2 SQUID on pulse-tube cryocooler, *Intermag Europe* GO-04.

[29] Ono, S., Kimura, M., Sekiya, N., Saito, A., Hirano, S., Ohshima, S., Harada, Y., Takahashi, T., Iriuda, H. & Yoshizawa, M. (2007). Design and fabrication of 5GHz miniaturized bandpass filters using superconducting microstrip quasi-spiral resonators, *IEEE. Trans. Appl. Supercond.* 17: 89.

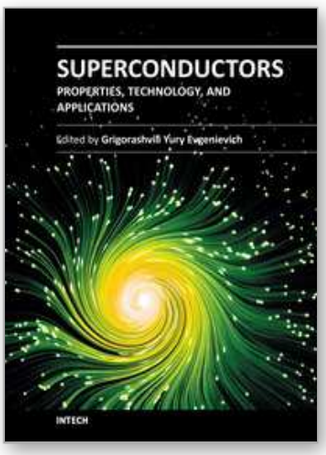

Superconductors - Properties, Technology, and Applications
Edited by Dr. Yury Grigorashvili

ISBN 978-953-51-0545-9
Hard cover, 436 pages
Publisher InTech
Published online 20, April, 2012
Published in print edition April, 2012

Book "Superconductors - Properties, Technology, and Applications" gives an overview of major problems encountered in this field of study. Most of the material presented in this book is the result of authors' own research that has been carried out over a long period of time. A number of chapters thoroughly describe the fundamental electrical and structural properties of the superconductors as well as the methods researching those properties. The sourcebook comprehensively covers the advanced techniques and concepts of superconductivity. It's intended for a wide range of readers.

InTech Europe
University Campus STeP Ri
Slavka Krautzeka 83/A
51000 Rijeka, Croatia
Phone: +385 (51) 770 447
Fax: +385 (51) 686 166
www.intechopen.com

InTech China
Unit 405, Office Block, Hotel Equatorial Shanghai
No.65, Yan An Road (West), Shanghai, 200040, China
中国上海市延安西路65号上海国际贵都大饭店办公楼405单元
Phone: +86-21-62489820
Fax: +86-21-62489821

IntechOpen